# The ciliary pocket: an endocytic membrane domain at the base of primary and motile cilia

**Anahi Molla-Herman[1,2,*], Rania Ghossoub[1,2,*], Thierry Blisnick[3,‡], Alice Meunier[4,‡], Catherine Serres[1,2], Flora Silbermann[5,6], Chris Emmerson[1,2], Kelly Romeo[1,2], Pierre Bourdoncle[1,2], Alain Schmitt[1,2], Sophie Saunier[5,6], Nathalie Spassky[4], Philippe Bastin[3] and Alexandre Benmerah[1,2,§]**

[1]Institut Cochin, Université Paris Descartes, CNRS UMR 8104, Paris 75014, France
[2]INSERM, U1016, Paris 75014, France
[3]Trypanosome Cell Biology Unit, Institut Pasteur and CNRS, Paris 75015, France
[4]Institut de Biologie de l'Ecole Normale Superieure (IBENS), INSERM U1024, CNRS UMR8197, Paris 75005, France
[5]INSERM, U983, Hôpital Necker-Enfants Malades, Paris 75015, France
[6]Université Paris Descartes, Paris 75006, France

*These authors contributed equally to this work
‡These authors contributed equally to this work
§Author for correspondence (alexandre.benmerah@inserm.fr)

*Accepted 4 March 2010*
*Journal of Cell Science 123, 1785-1795*

*doi:10.1242/jcs.059519*

## Summary

Cilia and flagella are eukaryotic organelles involved in multiple cellular functions. The primary cilium is generally non motile and found in numerous vertebrate cell types where it controls key signalling pathways. Despite a common architecture, ultrastructural data suggest some differences in their organisation. Here, we report the first detailed characterisation of the ciliary pocket, a depression of the plasma membrane in which the primary cilium is rooted. This structure is found at low frequency in kidney epithelial cells (IMCD3) but is associated with virtually all primary cilia in retinal pigment epithelial cells (RPE1). Transmission and scanning electron microscopy, immunofluorescence analysis and videomicroscopy revealed that the ciliary pocket establishes closed links with the actin-based cytoskeleton and that it is enriched in active and dynamic clathrin-coated pits. The existence of the ciliary pocket was confirmed in mouse tissues bearing primary cilia (cumulus), as well as motile cilia and flagella (ependymal cells and spermatids). The ciliary pocket shares striking morphological and functional similarities with the flagellar pocket of Trypanosomatids, a trafficking-specialised membrane domain at the base of the flagellum. Our data therefore highlight the conserved role of membrane trafficking in the vicinity of cilia.

**Key words:** Actin, Clathrin, Endocytosis, Flagellum, Motile cilia, Primary cilium

## Introduction

The primary cilium is a non-motile cilium whose axoneme is made of nine peripheral doublets of microtubules (9+0). This organisation is shared with motile cilia and flagella, which possess supplementary elements, such as dynein arms, radial spokes and a central pair of single microtubules (for a review, see Pedersen and Rosenbaum, 2008). Since the original discovery of the role of the primary cilium in polycystic kidney disease (Pazour et al., 2000), numerous studies have stressed the key function of cilia in the control of different physiological and developmental processes. These led to the concept that the primary cilium acts as a cellular antenna that senses the extracellular environment and translates these signals in specific intracellular signalling cascades (for reviews, see Christensen et al., 2007; Sharma et al., 2008).

Primary cilia are formed in quiescent cells from the mother centriole of the centrosome, which then becomes a basal body and nucleates the nine microtubule doublets forming the axoneme. Elongation of the organelle is ensured by intraflagellar transport (IFT), which trafficks axoneme precursors to the distal tip for construction (for reviews, see Pedersen and Rosenbaum, 2008; Scholey, 2008). Key transmission electron microscopy (TEM) studies were published by Sorokin in the 1960s, leading to the definition of two main different ciliogenesis pathways for primary cilia (Sorokin, 1962; Sorokin, 1968). In epithelial cells, the mother centriole appears to dock directly at the apical plasma membrane from where the 9+0 axoneme grows toward the extracellular milieu. The formation of motile cilia (9+2 axoneme) in multi-ciliated epithelial cells is thought to follow a similar pathway after the amplification of the basal bodies by the acentriolar pathway. By contrast, the cilium of fibroblasts or smooth muscle cells appears to grow within the cell body, upon docking of the mother centriole appendices to a vesicle of uncharacterised origin called the 'primary ciliary vesicle'. Growth of the axoneme takes place within this vesicle, which stretches to form the ciliary shaft and sheath. Fusion of this vesicle with the plasma membrane results in the emergence of the cilium in the extracellular environment.

However, TEM images indicate that the cilium can remain partially intracellular within a membrane invagination that is reminiscent to the flagellar pocket (FP) of Trypanosomatids, a family of flagellated protozoan parasites that are well known for causing tropical diseases such as sleeping sickness, leishmaniasis or Chagas disease. The FP is a membrane domain formed by an invagination of the plasma membrane that surrounds the base of the flagellum. It is the exclusive region for vesicular trafficking to and from the plasma membrane. Indeed, clathrin-coated pits were shown to form and to bud from the FP to form endocytic vesicles, a process by which plasma membrane proteins of the parasites are internalised (for reviews, see Field and Carrington, 2009; Overath and Engstler, 2004). The apparent structural similarity between the FP and the local organisation at the base of some cilia raises the

Journal of Cell Science

question of a functional similarity of these membrane domains. The existence of such a 'ciliary pocket' could be highly significant given the number of receptors that have been proposed to traffic between the cell body and the cilium.

In the present study, we investigated cilia structure and organisation in different model cell lines and in mouse tissues, using light microscopy and electron microscopy. Our data provide a thorough description of the ciliary pocket and reveal its interaction with the actin-based cytoskeleton. We also describe the presence of functional endocytic structures on this cilium-associated membrane domain, which, in addition to the structural similarity, demonstrate some functional relationships with the FP of Trypanosomatids.

## Results

### Structure of the primary cilium in epithelial kidney cells (IMCD3)

IMCD3 (Inner Medullar Collecting Duct) cells were used as a model to investigate the structure of the primary cilium in kidney epithelial cells. More than 90% of IMCD3 cells at 3 days post confluence assembled a single cilium detected by immunofluorescence (IF) using an antibody against acetylated-tubulin (AT, data not shown). Direct observation of the apical surface by scanning electron microscopy (SEM) revealed the presence of a cilium in 90% of the cells (Fig. 1A, arrows). IMCD3 cells harboured a single cilium of 2-5 μm, whose diameter narrowed progressively toward the distal tip (Fig. 1B,C). The majority of cilia emerged directly from the surface, in a similar manner to tree trunks from the ground (~89%, average of three experiments, *n*=226; Fig. 1B). However, a distinct profile was identified in the remaining population (~11%). The base of the cilium could not be visualised and the organelle seemed to emerge from a depression of the apical membrane (Fig. 1C).

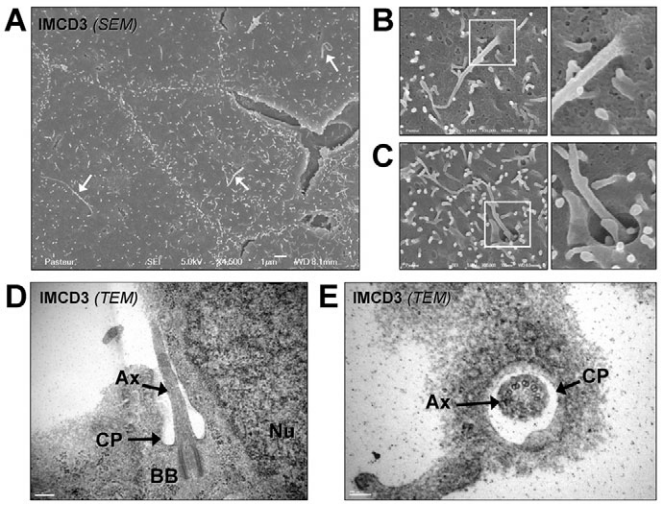


**Fig. 1. The presence of a ciliary pocket defines a minor population of primary cilia in IMCD3 cells.** IMCD3 cells were grown on coverslips 3 days post confluence, then fixed and treated for SEM (A-C) and TEM (D,E). SEM observations reveal the presence of a single cilium at the apical surface of IMCD3 cells (**A**, arrows) with a major population of cilia directly protruding from the plasma membrane (**B**) and a minor population of cilia emerging from an invagination of the membrane (**C**), consistent with the presence of a ciliary pocket. TEM images, longitudinal (**D**) and transverse (**E**) sections, confirm that cilia are found in an invagination of the plasma membrane, in agreement with SEM images. Axoneme (Ax), basal body (BB), ciliary pocket (CP) and nucleus (Nu) are indicated. Scale bars: 1 μm (A), 100 nm (B,C,E) and 200 nm (D).

Transmission electron microscopy (TEM) confirmed the presence of trunk-like cilia (data not shown), but also revealed that a few cilia were found in an invagination of the plasma membrane in both longitudinal (Fig. 1D) and cross-sections (Fig. 1E). The basal part of the cilium was found within the invagination, whereas the distal portion extended toward the surface of the cell. The basal body was localised just underneath the base of this depression.

Altogether, our data reveal that the basal part of the cilium can be localised within the lumen of what therefore looks like the flagellar pocket of trypanosomes (supplementary material Fig. S1) and hence was named the 'ciliary pocket'.

### Ultrastructural analysis of the ciliary pocket in RPE1 cells

To confirm these findings, we investigated another cell type: the telomerase-immortalised retinal pigment epithelial cell line (RPE1), one of the most popular models used to study primary cilia (Jurczyk et al., 2004). IF indicated that ~80% of RPE1 cells form a cilium when grown to confluence and maintained in low serum conditions (Molla-Herman et al., 2008). SEM analysis failed to detect cilia at the visible face of RPE1 cells (data not shown). We next turned to TEM, but initial analysis performed on transversal sections perpendicular to the adherent surface detected very few cilium profiles (data not shown).

We then used 3D reconstruction of deconvoluted epifluorescence images, a technique that allows the measurement of the length of axoneme, and also of its positioning. This revealed that cilia were not randomly positioned (data not shown) and that they were parallel to the adherent substrate lying on the cellular 'side'; this explains why they could not be detected by SEM. Hence, RPE1 cells were analysed by TEM with sections parallel to the adherent surface (Fig. 2A), which led to striking observations.

First, cilia were exclusively found within two or three consecutive sections, supporting the fact that they are not randomly positioned along the *Z*-axis. Second, most of the sections included the basal body and the proximal part of the axoneme of the same cilium, indicating that the organelle is indeed almost parallel to the section plane and therefore to the adherent surface. Finally, the basal body was deeply rooted within the cytoplasm, close to the nucleus, and docked at the bottom of a ciliary pocket. When the extracellular part of the cilium was visible, it emerged at the cell surface (Fig. 2B and data not shown), as observed in the minor population of IMCD3 cells (Fig. 1D).

Virtually all sections through cilia revealed this association, with an inverted-mushroom-shaped ciliary pocket that appeared symmetrical relative to the axis defined by the axoneme (Fig. 2C, green) and the mother centriole (red). The region corresponding to the pocket membrane surrounding the axoneme (Fig. 2C, blue) appeared to be variable in length. The cilium was released from its interaction with the invaginated plasma membrane and protruded at the surface of the cell (Fig. 2C).

### Characterisation of the ciliary pocket by immunofluorescence

To analyse the pocket by fluorescence microscopy, we set up an experimental system to allow the simultaneous visualisation of the plasma membrane and the cilium, plus any other marker. Several GFP fusions are currently used to stain the plasma membrane, we

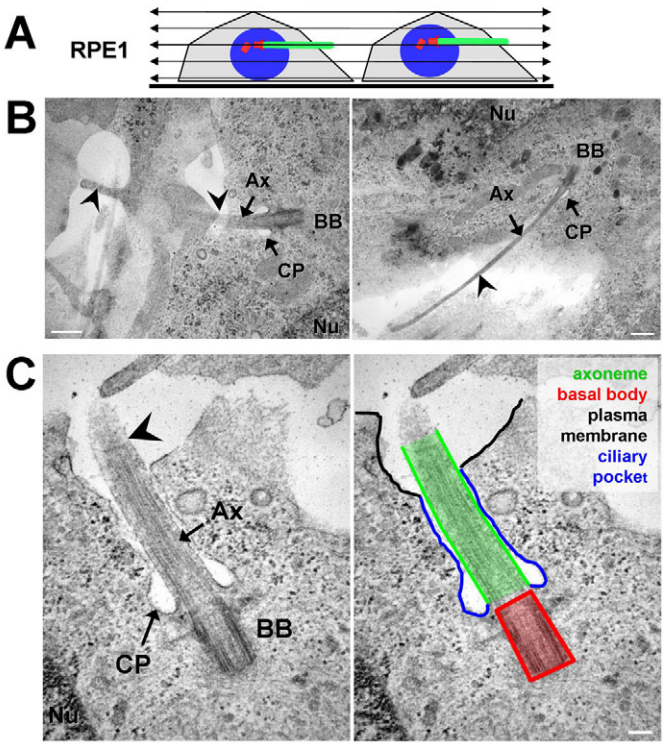


**Fig. 2. Transmission electron microscopy analysis of primary cilia in RPE1 cells.** RPE1 cells were grown on coverslips to confluence, then serum-starved, fixed and treated for TEM. (**A**) Sections were made parallel to the adherent surface, as depicted in the scheme. (**B**) Examples of cilia from cells starved for 24 (left) or 72 hours (right) in which both the basal body (BB) and the axoneme are clearly visible. (**C**) TEM images define the shape and membrane organisation of the ciliary pocket (CP) relative to the axoneme (Ax) and the basal body (BB). The different membranes and ciliary compartments are highlighted on the right. Extracellular distal part of the axoneme is indicated by an arrowhead. Scale bars: 500 nm (B), 100 nm (C).

therefore reasoned that they might also stain the membrane of the pocket, because the two membrane domains are continuous (Fig. 1D; Fig. 2C). Among the five constructs tested, the GFP fused to a farnesylation motif (GFP-F) gave the most interesting results. In ciliated RPE1 cells, the GFP-F signal was found all over the plasma membrane and appeared more intense around the AT staining, suggesting efficient targeting to the pocket and/or to the cilium (supplementary material Fig. S2A, arrow). This signal was specific, because it was not observed with a GFP fusion that was specific for early endosomal membranes (GFP-2xFYVE, supplementary material Fig. S2A). Furthermore, and as shown below, the shape and distribution of the ciliary pocket obtained with 3D reconstruction of deconvoluted images was fully compatible with our TEM results, indicating that GFP-F is a useful tool to stain the ciliary pocket.

### Actin filaments are present at the ciliary pocket

The characteristic shape of the ciliary pocket and the non-random positioning of cilia in RPE1 drove us to investigate cytoskeletal organisation at the pocket, including microtubules and actin. Analysis of TEM and epifluorescence images did not reveal any specific organisation of microtubules around the pocket. Microtubules were anchored to the basal body and from there appeared to spread in all directions all over the cytoplasm and around the nucleus (Fig. 3A and data not shown) with no specific or characteristic distribution at or around the cilium.

Thinner filaments whose diameter was compatible with actin filaments were observed beneath or above the ciliary pocket (Fig. 3A). RPE1 cells expressing the GFP-F fusion to stain the pocket membrane were stained for actin filaments using fluorescent phalloidin. Epifluorescence images and 3D reconstruction revealed the presence of actin filaments docked to the ciliary pocket (Fig. 3B). Although most cilia had actin filaments at the base of the pocket, some actin filaments were also observed along the rest of the cilium.

Actin dynamics at the pocket was analysed by live-cell fluorescence microscopy using well-characterised markers for the cilium (GFP-Rab8) and the actin filaments (LifeAct-Cherry) (Riedl et al., 2008). Control experiments showed that the Rab8 fusion stained cilia in RPE1 cells (supplementary material Fig. S2B) as described previously (Nachury et al., 2007; Yoshimura et al., 2007). LifeAct staining was very similar to that obtained using phalloidin in fixed cells (compare supplementary material Fig. S2C and Fig. 3B). As shown in Fig. 3D-F, the results obtained on live cells confirmed the interaction of actin filaments with the cilium. Filaments present at the base were stable (up to 20 minutes), which correlated with the absence of movement of the base of the cilium, whose position remained constant relative to the nucleus (data not shown). By contrast, actin filaments found at the middle and distal parts of the pocket were more dynamic (polymerisation and depolymerisation; Fig. 3D-F and supplementary material Movies 1-4). Interestingly, sites of actin dynamics often corresponded to the deformation of the axoneme, including bending or tightening (Fig. 3E,F and supplementary material Movies 2-4).

Altogether, these results show that the ciliary pocket is closely associated with stable and dynamic actin filaments, which might act on both the positioning and function of the cilium.

### Clathrin-coated pits are present at the ciliary pocket

As indicated above, the ciliary pocket resembled the flagellar pocket of trypanosomes (compare Fig. 1D and Fig. 2C with supplementary material Fig. S1A), a membrane domain that is specialised in vesicular trafficking (supplementary material Fig. S1B). We therefore investigated whether the ciliary pocket was involved in vesicular-trafficking activity. Strikingly, TEM images demonstrated that the region of the ciliary pocket often presents typical invaginated profiles with electron-dense indented material at the cytoplasmic side of the membrane (Fig. 4A-C), which is characteristic of the clathrin coat, therefore suggesting the presence of clathrin-coated pits (CCPs).

Ciliary-pocket-associated CCPs were further characterised by IF, revealing the presence of the clathrin-adaptor complex AP-2 (Fig. 4D), as well as epsin, Eps15 and CALM (data not shown), which are standard markers of CCPs. Although these spots were in close proximity to the cilium, it was difficult to discriminate between plasma membrane or ciliary pocket localisation. We used the GFP-F fusion and 3D reconstruction to resolve this issue. RPE1 cells transiently expressing GFP-F were stained for the AP-2 complex and for AT. AP-2-positive spots were found along AT- and GFP-F-positive signals (Fig. 4D), suggesting localisation to the membrane of the pocket. 3D reconstruction clearly demonstrated the presence of CCPs budding from the ciliary pocket decorated by GFP-F (Fig. 4E), in agreement with the global

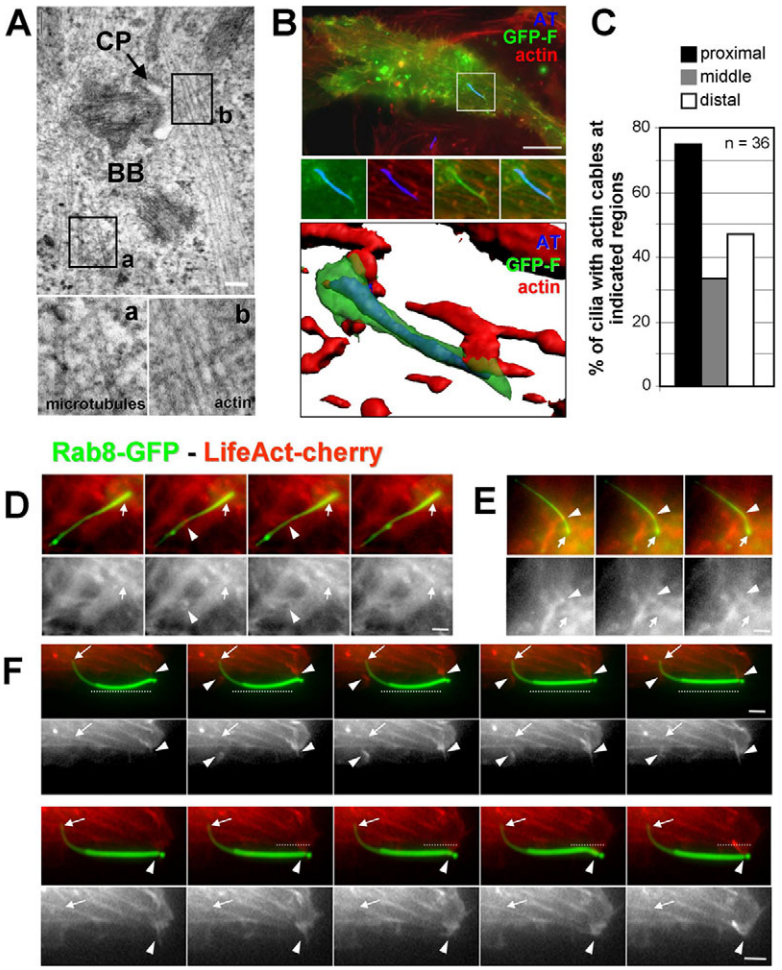


**Fig. 3. The ciliary pocket is a docking site for actin filaments.** (**A**) TEM analysis of RPE1 cells shows two types of filaments close to the ciliary pocket (CP), including thick filaments (~21 nm) and thinner ones (~6 nm), which probably correspond to microtubules (a) and actin (b), respectively. (**B**) RPE1 cells transiently expressing GFP-F, were serum-starved for 24 hours and processed for IF. Cilia and filamentous actin were stained using antibody against AT (blue) and phalloidin (red), respectively. 3D reconstruction of the same cell indicates that the GFP-F fusion (green) stains a membrane domain around the axoneme (blue) where actin filaments (red) appear to dock. (**C**) 3D images to analyse the distribution of actin filaments relative to cilium subdomains. Results are expressed as the number of cilia with actin filaments at the indicated regions. Scale bars: 100 nm (A) and 5 μm (B). (**D-F**) RPE1 cells transiently co-transfected with rab8-GFP (green) and LifeAct-Cherry (red), were serum-starved for 48 hours and analysed by live-cell fluorescence microscopy (37°C; one picture every 5 seconds for 3 minutes). Three representative examples are shown as image streams (1 image every 20 seconds). Actin filaments or cables (arrows) are docked at the base of cilia and actin remodelling (arrowheads) occurs at the middle or distal part of cilia. Dotted white lines denote modifications of the cilium. Scale bars: 1 μm.

organisation of the pocket membrane and the distribution of CCPs observed by TEM (Figs 2 and 4).

3D reconstruction was also used to analyse the localisation of CCPs along the pocket that was arbitrarily divided into three equal portions of the axoneme (proximal, middle and distal; Fig. 4E). This analysis revealed an average number of 5.3±3.4 CCPs per pocket ($n$=40), with CCPs preferentially found around the proximal region of the axoneme, a result that was again fully compatible with the TEM images (Fig. 4 and data not shown). The fact that we could easily identify CCP profiles at the ciliary pocket by TEM suggested an enrichment of these structures, because few CCP profiles were detected on the rest of the plasma membrane (data not shown). We then examined the surface of the pocket by TEM and 3D reconstruction to evaluate the density of CCPs. There were ~3 times more CCPs per surface unit at the pocket membrane compared with the rest of the plasma membrane (supplementary material Fig. S3). In summary, these results show that the ciliary pocket is likely to be an endocytic compartment that is enriched in CCPs.

### Clathrin-dependent endocytosis is not required for ciliogenesis

To investigate the role of CCPs at the ciliary pocket, RNA interference was carried out to knock down the AP-2 complex, which specifically and drastically affects the formation of CCPs (>90% inhibition), resulting in a strong and specific inhibition of clathrin-dependent endocytosis and not of other clathrin-mediated processes (Hinrichsen et al., 2003; Motley et al., 2003).

The AP-2 complex is composed of four different subunits (α-adaptin, β2, μ2 and σ2) and targeted depletion of a single subunit leads to the degradation of the whole complex (Borck et al., 2008; Hinrichsen et al., 2003; Motley et al., 2003). Depletion of the AP-2 complex in RPE1 cells using siRNA to knock down α-adaptin was checked by western blot (Fig. 5A) and confirmed by IF (Fig. 5B). Importantly, ciliogenesis was induced by serum starvation 2 days after siRNA transfection. Despite efficient depletion of AP-2, ciliogenesis was not affected; 80% of cells possessed a single rod-like AT staining, a percentage that was similar to that in cells treated with control siRNA (Fig. 5B,C). Since clathrin-dependent and AP-2-independent internalisation events have been described (Hinrichsen et al., 2003; Motley et al., 2003), we also investigated the consequences of depletion of the clathrin heavy chain. Despite efficient depletion of clathrin (Fig. 5A,B), ciliogenesis was only moderately affected (20% inhibition, Fig. 5C).

TEM analysis of AP-2-depleted cells (Fig. 5D) or cells treated with Dynasore (data not shown), a drug that inhibits dynamin and therefore clathrin-coated vesicle (CCV) formation (Macia et al., 2006), did not reveal striking modification of the ciliary pocket. However, uncoated budding profiles smaller than CCPs were observed at the pocket in AP-2-depleted cells (Fig. 5D, arrowheads),

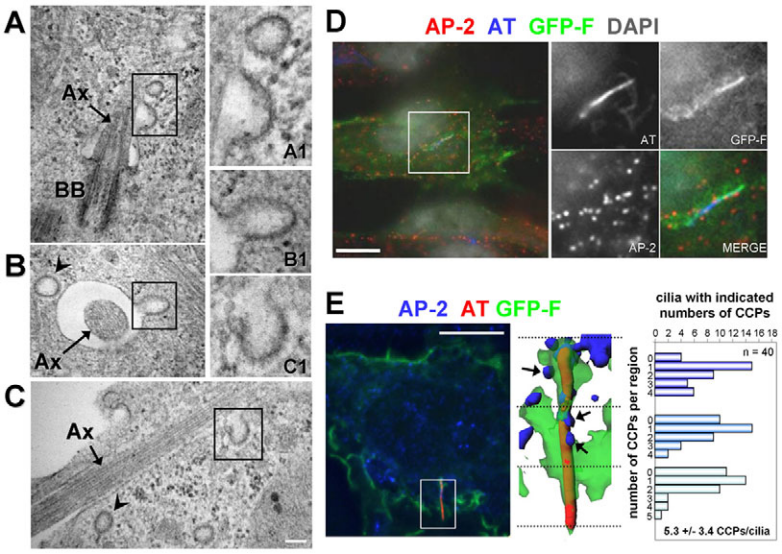


**Fig. 4. Characterisation and distribution of clathrin-coated pits at the ciliary pocket.** RPE1 cells were processed for TEM as in Fig. 2. Representative images of cilia with characteristic clathrin-coated profiles are shown (**A-C**). Sections of clathrin-coated pits are enlarged in A1-C1. Axoneme (Ax, arrows) and basal body (BB) are indicated. (**D**,**E**) RPE1 cells transiently transfected with GFP-F, were serum-starved for 24 hours and then processed for IF. Cilia and CCPs were stained using antibodies against AT and AP-2 complex, respectively, whereas nuclei were stained using DAPI, as indicated. GFP-F (green) stained the plasma membrane and the staining appeared brighter at the cilium. (E) Deconvoluted images (left) and 3D images (middle) indicated that GFP-F (green) stained a membrane domain around the proximal and middle regions of the axoneme (red) where cilium-associated CCPs (blue, arrows) are found. 3D images were used to analyse the number and distribution of cilia-associated CCPs relative to cilium subdomains, including the proximal, middle and distal domains of the axoneme. Results are expressed as the number of cilia with the indicated number of CCPs per cilium region. Scale bars: 100 nm (A-C), 5 μm (D,E).

suggesting that a clathrin-independent pathway compensates for the absence of functional CCPs. These results indicate that clathrin-mediated endocytosis is not required for the assembly or the maintenance of the primary cilium.

### CCPs associated with the ciliary pocket are active endocytic structures

The presence of CCPs does not necessarily mean that they are functional and/or able to form CCVs (supplementary material Fig. S4A). To evaluate the possible endocytic activity of ciliary-pocket-associated CCPs, RPE1 cells transiently expressing the GFP-F fusion were incubated for 2 minutes at 37°C with fluorescent transferrin, a marker of clathrin-dependent endocytosis (for a review, see Benmerah and Lamaze, 2007). Similarly to plasma membrane CCPs, pocket-associated CCPs were efficiently stained with transferrin (Fig. 6A,B), indicating that they are active endocytosis sites.

To demonstrate that these CCPs were dynamic, we examined rab8-GFP and clathrin light chain labelled with DsRed (clathrin-DsRed) (Rappoport et al., 2003) in live cells. Preliminary experiments carried out in fixed cells revealed the presence of clathrin-DsRed at the plasma membrane and at the *trans*-Golgi network (TGN) close to the basal body, and in spots colocalising with AP-2 around the cilium (supplementary material Fig. S4B and data not shown), a distribution which matches that of endogenous clathrin heavy chain. Co-expression of rab8-GFP with clathrin-DsRed showed numerous clathrin spots tightly associated with and all along the proximal and middle part of the ciliary pocket (Fig. 6C), in agreement with results observed in fixed cells (supplementary material Fig. S4B). Clathrin-DsRed also decorated larger structures around the basal body and the proximal region of the cilium (Fig. 6C), which probably correspond to clathrin coats found at the TGN. Direct videomicroscopy revealed highly heterogeneous dynamics for cilia-associated clathrin. Some spots close to the basal body appeared rather static, whereas others seemed to scan the surface of the cilium. In some cases, vesicles coming from the cytoplasm were found to dock to the ciliary pocket (data not shown). Other movements correspond to internalisation events, i.e. transformation of a CCP into a CCV that detached from the ciliary pocket region and then moved deeper in the cytoplasm, as classically observed at the plasma membrane (Rappoport et al., 2004) (supplementary material Fig. S4A). These spots were initially 'attached' to or in close contact with the cilium and therefore could correspond to pre-formed CCPs. Their disappearance could be explained by movement of the formed CCVs into the cytoplasm, hence leaving the focal plane, but could also correspond to uncoating of the clathrin coat from the formed vesicle (supplementary material Fig. S4A), resulting in the loss of clathrin-DsRed staining. An example of such a spot is shown as an image stream at Fig. 6D and in supplementary material Movie 5, in which several examples of CCV formation from a single cilium were observed (arrows). These results clearly indicate that the ciliary pocket is able to form CCVs.

### The ciliary pocket is present in several types of ciliated cell

To determine the importance of the ciliary pocket, other cell types were investigated. The presence of the pocket was shown in cultured cell lines such as IMCD3 cells (Fig. 1). Murine embryonic fibroblasts (MEFs) also form primary cilia in vitro in low serum conditions (Molla-Herman et al., 2008) (supplementary material Fig. S5C), which we also found within a pocket (supplementary material Fig. S5C). In both cases, CCPs were also detected at the pocket (supplementary material Fig. S5, arrowheads).

We then investigated the presence of the pocket in vivo, as suggested in previously published images (see Discussion). First, we took advantage of ongoing studies on oocytes from ovulating mice to investigate cilia in cells from the cumulus. A centrally located cilium has been identified in granulosa cells (Herman and Albertini, 1983) and in non-dividing mural and cumulus granulosa cells of antral follicules (Teilmann et al., 2005). To our knowledge, it was not clear whether the cilium persists in cumulus cells after ovulation. Using TEM, we found primary cilia emerging from a pocket (Fig. 7A,B). CCPs were also found to bud from the pocket membrane (Fig. 7C, arrowheads), demonstrating structural and functional similarities with pockets in RPE1 cells.

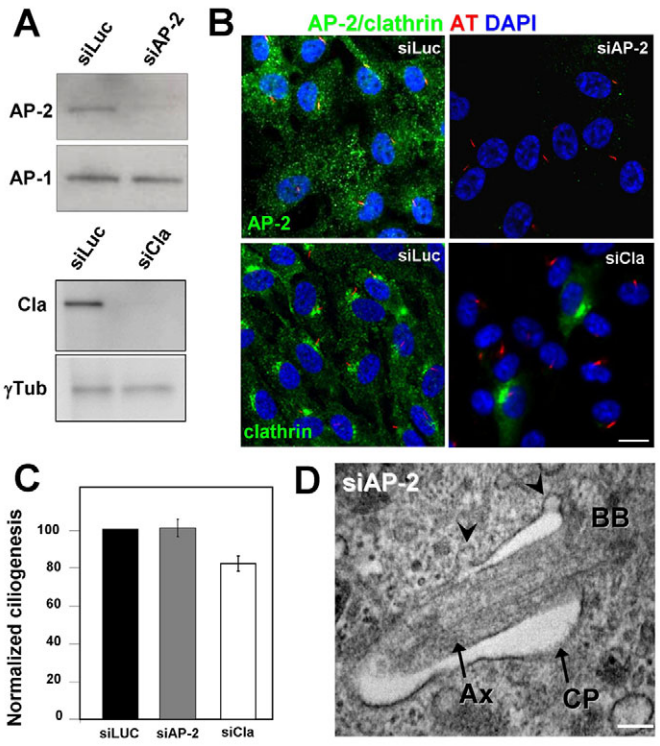


**Fig. 5. Clathrin-mediated endocytosis is not required for ciliogenesis.** (**A**) RPE1 cells were treated with siRNA to knock down luciferase (siLuc, as a control), α-adaptin (siAP-2) or clathrin heavy chain (siCla) and analysed by western blot using antibodies against α-adaptin (AP-2) or clathrin (Cla), and γ-adaptin (AP-1) or γ-tubulin (γTub), as controls, respectively. (**B**) The ability of siRNA-treated RPE1 cells to form primary cilia was analysed by IF using antibodies against AP-2 or clathrin (green) and AT (red). Nuclei were stained with DAPI. (**C**) Results in B were quantified and expressed as normalised ciliogenesis corresponding to the proportion of cells with a single rod-like AT positive structure ($n$>700 cells, three independent experiments) relative to siLuc treated cells (100%). (**D**) RPE1 cells treated with α-adaptin targeting siRNA, were fixed and treated for TEM as in Fig. 2. Uncoated budding profiles at the ciliary pocket (CP) are indicated by arrowheads. Ax, axoneme. Scale bars: 5 μm (B), 100 nm (D).

Next, we investigated whether the presence of a pocket could be extended to motile cilia. As a model cellular system we used 9+2 motile cilia from ependymal cells of the developing brain in mice. These multi-ciliated cells cover the ventricular cavities and the beating of their cilia is required to propel the cerebrospinal fluid. SEM analysis of these cells showed that they displayed about 50 cilia at their apical surface (data not shown). TEM analysis of in vitro (Fig. 7D) and in vivo (Fig. 7E) maturing ependymal cells revealed that the base of motile cilia was also found within a pocket that could, however, contain one to several (<10) cilia (Fig. 7D,E). Dense networks of actin filaments were found close to the pocket (Fig. 7D). In addition, we frequently observed CCPs budding from the pocket membrane toward the cytoplasm (Fig. 7D,E; arrowheads), stressing once more endocytic activity of the ciliary pocket.

In conclusion, the ciliary pocket is present at the base of both primary and motile cilia and is not limited to cultured cells. The presence of CCPs in the ciliary pocket and its localisation next to the actin network provide evidence for a highly organised microdomain associated with cilia.

## Discussion

This study defines and characterises the ciliary pocket, a membrane domain found at the base of different types of cilia, which exhibits endocytic activity and interacts with the actin-based cytoskeleton.

### The ciliary pocket: characterisation and cell-type specificities

The ciliary pocket is defined as an invagination of the plasma membrane found at the ciliary base (Fig. 8A). This morphological definition is based on detailed ultrastructural analysis of two established cell lines, RPE1 and IMCD3 cells. It fits with images found in published TEM studies, where a morphologically similar membrane domain is visible in many different cell types such as fibroblasts (Sorokin, 1962; Wheatley, 1969), smooth muscle cells (Sorokin, 1962), mesenchyme limb bud cells (Fonte et al., 1971), chondrocytes (Jensen et al., 2004), gingival cells (Nikai et al., 1970), secretory cells of the adenohypophysis (Dingemans, 1969), keratocytes (Smith et al., 1969) and neurons (Brechbuhl et al., 2008; Breunig et al., 2008; Han et al., 2008). We show the presence of a ciliary pocket in cells from the cumulus around ovulated oocytes (Fig. 7A-C). The pocket is therefore a membrane domain commonly found at the base of primary cilia.

The presence of a ciliary pocket in non-epithelial cells is in agreement with Sorokin's model of ciliogenesis in these cells. In this 'intracellular' pathway (Fig. 8B), the axoneme grows in the cytoplasm within the elongating primary ciliary vesicle that is docked onto the mother centriole. The formation of a ciliary pocket would correspond to the fusion between the sheath and the plasma membrane, leading to the emergence of the cilium in the extracellular milieu. Therefore, the ciliary pocket could be a transitory structure present only in cells with a non-mature primary cilium that is still under construction. We do not favour this hypothesis for several reasons. First, cilia rooted in a pocket were equally abundant in RPE1 cells in which ciliogenesis had been induced for increasing periods (72 vs 24 hours, Fig. 2B right and data not shown). Second, all cilia in cells of the cumulus, which are non-dividing differentiated cells, were also found deeply rooted in a ciliary pocket. Altogether, these data indicate that the ciliary pocket is unlikely to reflect only intermediate stages in ciliary formation.

The presence of a pocket in a minor population of primary cilia in kidney epithelial cells (IMCD3) was not expected because ciliogenesis in these cells is thought to occur by direct docking of the mother centriole at the apical membrane from where the cilium grows extracellularly (Fig. 8B). This could be explained by several hypotheses: (1) a ciliary pocket could form as the consequence of a 'retraction' of the basal body deeper into the cytoplasm, in a post-assembly process (Sorokin, 1968); (2) only a minor population of IMCD3 cells follow the intracellular assembly route; or (3) all cells follow the intracellular pathway, but with faster kinetics than in non-polarised cells, including limited intracellular growth of the axoneme followed by a rapid fusion of the sheath with the plasma membrane and a complete and rapid protrusion of the cilium. Accordingly, Sorokin noticed such a heterogeneity in lung epithelial cells, which showed the presence of basal bodies with docked primary ciliary vesicles very close to the apical membrane and/or cilia with small ciliary-pocket-like structures (Sorokin, 1968).

The presence of a ciliary pocket in ependymal cells is unexpected because their motile cilia directly emerge from the apical membrane in mature tissues (Mirzadeh et al., 2008) (data not shown). The pocket looks quite similar to those of primary cilia, except for the

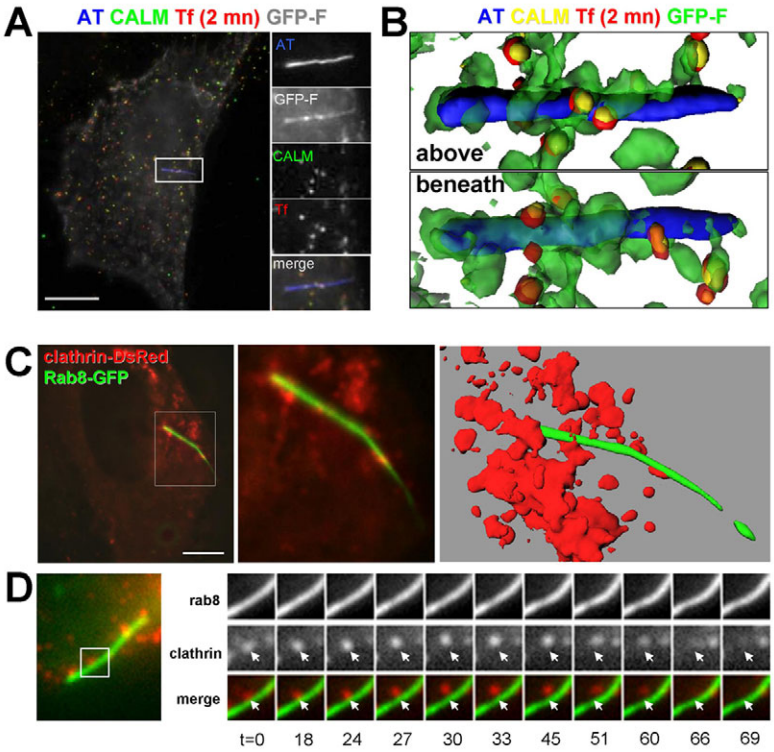


**Fig. 6. Ciliary-pocket-associated CCPs are active sites of endocytosis.** RPE1 cells were transiently transfected with the GFP-F encoding plasmid, incubated 2 minutes at 37°C with Alexa Fluor 555-conjugated transferrin (Tf, red). Cells were immediately fixed and processed for IF using antibodies against AT to stain the axoneme (blue), and CALM (yellow) to stain CCPs. Epifluorescence (**A**) and 3D reconstruction (**B**) images of a representative cilium containing region is shown. (B) Ciliary-pocket-associated CCPs stained for both CALM (yellow) and Tf (red). (**C**,**D**) RPE1 cells transiently co-transfected with plasmids encoding for rab8-GFP (green) or clathrin-DsRed (red) fusions analysed by live-cell fluorescence microscopy. (C) Live cells were imaged at 20°C to slow down clathrin dynamics to allow 3D analysis. Deconvoluted images (left) and 3D reconstruction (right) of the cilium-containing region of a representative cell are shown. (D) Live cells were imaged at 37°C (one image for each colour every 3 seconds for 4 minutes). The first image is shown (left). An image stream of a clathrin spot, which disappeared during the acquisition is shown (right, time is in seconds). The initial position of the followed clathrin spot is indicated with an arrow. Scale bars: 5 µm.

presence of several cilia, possibly as a result of the fusion of several pockets containing a unique cilium or of the growth of multiple cilia into the same vesicle (Fig. 7D,E). Therefore, these cilia could also follow the intracellular pathway for assembly and correspond to immature stages of development. This is in agreement with multiciliated cells of the *Xenopus laevis* epidermis, where docking of the basal body to apically located vesicles is required for ciliogenesis (Park et al., 2008). Alternatively, this could illustrate specific functions for these cilia and the ciliary pocket that are not required in adulthood.

In differentiating spermatids, the flagellum is found within an invagination of the plasma membrane. This structure is transient; the base of the pocket of the flagellum detaches from the basal body and migrates toward the tip of the axoneme to form the junction of the middle and the principal pieces in late spermatids (Fawcett et al., 1970). Our TEM analysis of spermatids indeed confirmed the presence of a deep invagination of the plasma membrane around the proximal part of the axoneme (supplementary material Fig. S6). Similarly to motile cilia, a ciliary pocket is present at the base of the flagellum during its maturation process.

In conclusion, these results indicate that the ciliary pocket could reflect intermediate stages of cilia formation. However, its wide presence at primary cilia in several cell types at advanced stages of their lives raises the issue of its specific functions.

### The ciliary pocket: structure and possible functions?

A first common feature for a specific functional role of the ciliary pocket is the presence of CCPs at the cytoplasmic side of the membrane, as suggested by TEM studies of chondrocytes or mesenchyme cells from the limb bud (Fonte et al., 1971; Haycraft et al., 2005; Jensen et al., 2004). Moreover, whereas CCP budding profiles by TEM were rare events at the plasma membrane, CCPs are found at relatively high density at the pocket, arguing for active trafficking. Our analysis demonstrates the molecular composition of these CCPs, their ability to concentrate cargo (transferrin) and their dynamics during budding and fission events (Figs 4, 6). This raises the issue of the nature of the receptor-ligand complexes present at the ciliary pocket.

A second common feature is the interaction with the actin cytoskeleton. In motile cilia, a connection between the basal body region and the apical actin cables is proposed to be involved in migration of the basal body to the membrane (for a review, see Vladar and Axelrod, 2008). This could participate in positioning of the cilium, as suggested by preliminary results indicating that disruption of actin cables results in mispositioning and deformation of primary cilia in RPE1 cells (R.G. and A.B., unpublished observations). Dynamic actin remodelling occurs along the cilium and is correlated with deformation or curvature of the organelle (Fig. 3E,F). This could have another function, such as transmission of mechanical stress to the cilium. Interestingly, in elongating spermatids, the pocket is a specific site for docking of chromatoid bodies and material involved in the assembly of the future annulus. The annulus is a septin-based cytoskeletal structure that migrates with the base of the membrane of the pocket to reach its definitive position, just distal to the last mitochondria of the middle piece (Ihara et al., 2005; Kissel et al., 2005). Remarkably, septins are known to interact with actin (Spiliotis and Nelson, 2006). Altogether, our observations favour a shared role of the ciliary pocket as an actin-cilium interface organelle.

### Does the ciliary pocket resemble the Trypanosomatid flagellar pocket?

The ciliary pocket shares intriguing relationships with the FP of Trypanosomatids: the general morphology, the presence of coated pits, the trafficking activity and an association with the actin cytoskeleton (for a review, see Field and Carrington, 2009). In

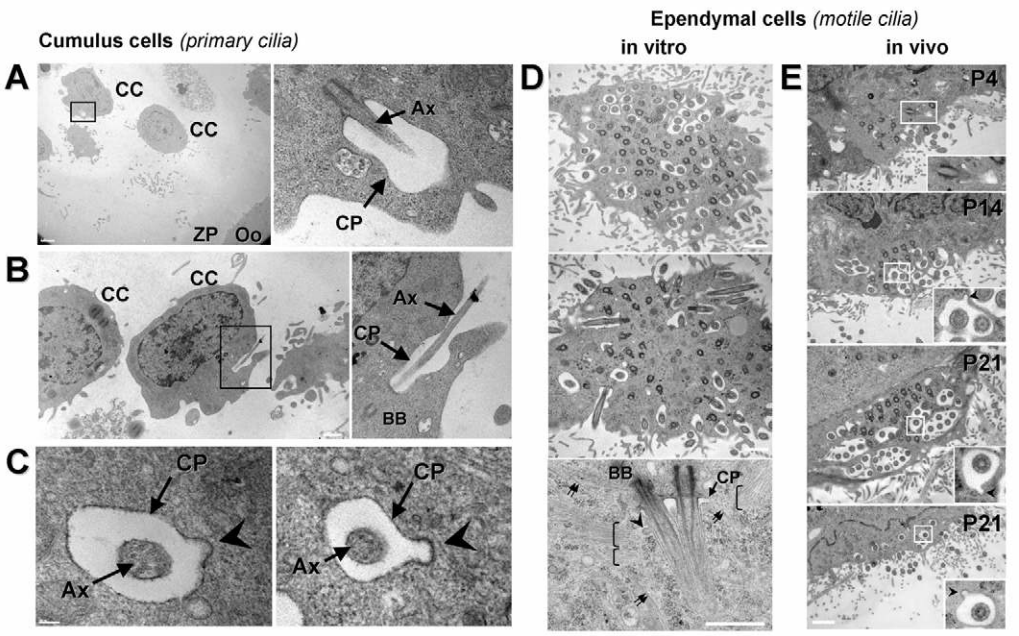


**Fig. 7. Presence of cilia-associated ciliary pockets in cumulus cells and ependymal multiciliated cells.** (**A-C**) Oocyte-cumulus complexes were collected from hyper-ovulating mice. (A) A low magnification TEM image of the cumulus-oocyte complex shows the cumulus cells and their ramifications embedded in an extracellular matrix around the zona-pellucida–oocyte complex. These cells possess single cilia within a ciliary pocket (black box). On an enlarged view of this region, the basal body and the proximal region of the axoneme within the pocket were clearly identifiable. (B) Another example with a cilium emerging in the extracellular media from a ciliary pocket. (C) Transverse sections of cilia show the axoneme inside a pocket and electron-dense indented profiles characteristic of CCPs budding from the membrane of the pocket (arrowheads). Cumulus cells (CC), Zona pellucida (ZP), oocyte (Oo), basal body (BB), Axoneme (Ax), Ciliary pocket (CP). (**D**) Ependymal cells differentiated in vitro, fixed and analysed by TEM. Sections from three different cells are shown in which the proximal region of motile 9+2 cilia are found within a pocket. In the bottom image, double arrows and brackets highlight microtubules and actin filaments, respectively. Ciliary pocket (CP), basal body (BB) as well as a CCP profile (arrowhead) are also indicated. (**E**) Ventricles of P4, P14 and P21 mice analysed by TEM. Motile cilia are found within pockets that can contain one to several cilia. Arrowheads indicate CCP budding from pockets. Scale bars: 2 µm (A), 1 µm (B,D,E), 100 nm (C).

trypanosomes, CCPs at the FP mediate the internalisation of plasma membrane proteins. We show here that this is also the case for transferrin (Fig. 6A,B), a basic marker for clathrin-dependent endocytosis. In contrast to Trypanosomatids, where budding takes place at a specific sub-localisation of the FP (Gadelha et al., 2009), CCPs are detected over the whole surface of the ciliary pocket (Fig. 4). This could be related to the extremely polarised trafficking at the FP, which is the only site for endocytosis and exocytosis in Trypanosomatids. This is not the case in the cell types studied here, and the contribution of the ciliary pocket to the overall endocytosis

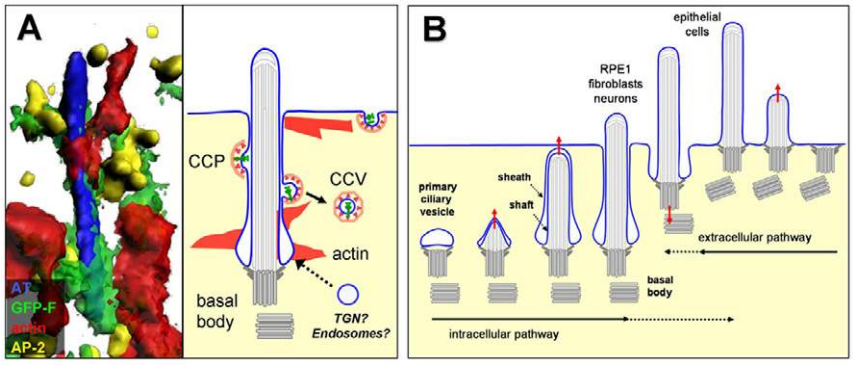


**Fig. 8. Cell-type-dependent ciliogenesis pathway and ciliary-pocket-associated vesicular trafficking.** (**A**) A 3D reconstruction of a representative RPE1 cell primary cilium showing the axoneme (blue), the ciliary pocket (green), actin filaments (red) and CCPs (yellow). The ciliary pocket is an endocytic membrane domain from where clathrin-coated vesicles are formed, which is also involved in the interaction with the actin-based cytoskeleton. We propose that it could also serve as a platform for the docking of vesicles coming from the secretory pathway or from endosomes. (**B**) In the intracellular pathway (left), a primary ciliary vesicle first interacts with the mother centriole, the axoneme then grows within this vesicle forming then the shaft and the sheath. The latter eventually fuses with the plasma membrane, allowing the distal part of the cilia to interact with the extracellular milieu. In the extracellular pathway (right), the mother centriole directly docks to the plasma membrane, with the cilium growing directly in the extracellular milieu.

is probably limited. However, the high density of CCPs at the ciliary pocket suggests that it could mediate internalisation of proteins from the ciliary membrane. This could be relevant for G-protein-coupled receptors such as smoothened or the somatostatin type-3 receptor, which are both targeted to the primary cilium (Corbit et al., 2005; Schulz et al., 2000) and regulated by endocytosis at the plasma membrane of non-ciliated cells (Chen et al., 2004; Kreuzer et al., 2001). However, despite our efforts, we failed to detect these receptors in ciliary-pocket-associated CCPs, even upon agonist activation (data not shown) (Molla-Herman et al., 2008).

The absence of clathrin in trypanosomes results in a 'big-eye' phenotype, where the FP enlarges massively as a result of inhibition of endocytosis and the continuous delivery of material (Allen et al., 2003). This phenotype is due to the presence of a cytoskeletal collar at the tip of the FP (supplementary material Fig. S1), which prevents exchange with the rest of the cell surface. Such a structure was not found at the ciliary pocket, in agreement with the lack of homologues of the only known molecular component of the FP collar in mammals (Bonhivers et al., 2008). Accordingly, a big-eye phenotype was not observed when clathrin-mediated endocytosis was functionally knocked down in RPE1 cells. Finally, in both trypanosomes and RPE1 cells, inhibition of clathrin did not interfere with construction of the flagellum (Allen et al., 2003) or of the cilium (Fig. 5).

Actin is found at the surface of the FP, and its depletion also resulted in a big-eye phenotype, indicating an involvement in CCV formation (Garcia-Salcedo et al., 2004). This might also be the case in mammalian cells, where actin polymerisation is known to be associated with the formation of CCVs (for a review, see Perrais and Merrifield, 2005). Finally, the ciliary pocket could behave as a docking platform for incoming vesicles that would specifically bring new membrane proteins to be incorporated into the ciliary membrane (Fig. 8A). In this situation, the presence of CCPs would be involved in the removal of excess membranes and/or of membrane proteins, to maintain the overall organisation of this intriguing domain.

## Materials and Methods

### Plasmids, antibodies and reagents

The pEGFP-F plasmid encodes farnesylated green fluorescent protein (GFP-F), a modified form of GFP that is targeted to the plasma membrane (Clontech). The plasmid encoding a fusion of clathrin light chain and DsRed (clathrin-DsRed) was described previously (Rappoport et al., 2003). The plasmids encoding Rab8-GFP and the LifeAct-Cherry (Riedl et al., 2008) were generous gifts of Arnaud Echard and Guillaume Montagnac (Institut Curie, Paris, France).

Rabbit polyclonal antibodies against Pericentrin (ab4448) and clathrin heavy chain (ab21679) were from Abcam. Mouse monoclonal antibodies against acetylated tubulin (clone 6-11B-1), α-tubulin (DM1A), γ-tubulin (GTU88) and γ-adaptin subunit of the AP-1 clathrin adaptor complex (clone 100.3) were from Sigma. Rabbit polyclonal antibodies against the α-adaptin subunit of the AP-2 clathrin adaptor complex (sc-10761) and goat polyclonal antibodies against CALM (sc-6463), epsin (sc-8673) and Eps15 (sc-11716) were from Santa Cruz Biotechnology. Alexa Fluor 555-conjugated transferrin and Alexa Fluor 546-conjugated phalloidin were from Molecular Probes (Invitrogen). Horseradish-peroxidase-conjugated donkey anti-rabbit or anti-mouse IgG were from Jackson ImmunoResearch.

### Animals

Pubertal C56BL/6 female mice were superovulated by the intraperitoneal injection of 5 IU of pregnant mare serum gonadotropin (PMSG, Folligon, Intervet) followed by 5 IU of human chorionic gonadotropin (hCG, Chorulon, Intervet) 48 hours later. Mice were killed by cervical dislocation and the cumulus-oocyte complexes (COCs) were collected from the oviduct in a drop of ferticult IVF medium (FertiPro N.V., Belgium), 14 hours after the hCG injection. C57BL/6 adult male mice were anaesthetised with $CO_2$ and killed by cervical dislocation and the testis were collected and washed in PBS. For ependymal cells studies, P4, P14 or P21 OF-1 mice (for in vitro and in vivo experiments respectively) were anaesthetised with $CO_2$ and killed by decapitation. Brains were then removed and washed in PBS. All the experimental procedures were conducted in accordance with the policies of the University and the Guidelines for biomedical research involving animals.

### Cells

RPE1, a human retinal pigment epithelial cell line that stably expresses human telomerase reverse transcriptase (hTERT-RPE1; Clontech) was a kind gift from Michel Bornens (Institut Curie, Paris, France). Inner medullar collecting duct cells (IMCD3) were from ATCC. Mouse embryonic fibroblasts (MEFs) from wild-type mice were a kind gift of Robert J. Lefkowitz (Howard Hughes Medical Institute, Durham, NC). Cells were grown in Dulbecco's modified Eagle's medium DMEM-F12 1:1 (IMCD3 or RPE1) or DMEM (MEF) supplemented by 10% fetal bovine serum (FBS, Invitrogen) for basic cell culture conditions. To induce ciliogenesis, IMCD3 cells were grown to confluence on coverslips in basic cell culture conditions and then maintained in the same conditions for additional 24, 48, 72 or 96 hours. To induce ciliogenesis in RPE1 cells, cells were grown to confluence on coverslips in basic cell culture conditions and then transferred in low-serum medium (0.5% FBS) for an additional 24 hours, as previously described (Molla-Herman et al., 2008). Cells from the subventricular zone of newborn mice were dissociated, resuspended in fresh medium, plated at high density in 10% FCS containing medium, and allowed to grow to confluence. Pure confluent astroglial monolayers were plated at a density of $7\times10^4$ cells/cm$^2$ and maintained in serum-free medium for ependymal differentiation for 5 days.

### Transfection

Transfections were done following the recommended procedure of the FuGENE HD (Roche) transfection reagent. Subconfluent RPE1 and IMCD3 cells grown on coverslips or in μ-slides (Ibidi) for live-cell imaging were transfected and immediately transferred to low-serum conditions for 24 hours for RPE1 cells or grown for additional 24 or 48 hours in basic conditions for IMCD cells.

For knockdown experiments, RPE1 cells were treated with control siRNA (5′-GCC ATT CTA TCC TCT AGA GGA TG-3′) or with siRNA targeting the AP-2 complex (5′-GAG CCG ACA CCA CCG CCA U-3′) or clathrin heavy chain (5′-AAC CUG CGG UCU GGA GUC AAC-3′), as previously described (Borck et al., 2008; Huang et al., 2004; Molla-Herman et al., 2008). Briefly, siRNA duplexes (Dharmacon or Eurogentec) were transfected using Oligofectamine RNAiMAX transfection reagent (Invitrogen) according to the manufacturer's instructions. Subconfluent RPE1 cells were transfected on the first day with 12 pmol siRNA. Transfected cells were transferred to low-serum medium (0 or 0.5%) on day 3 or day 4 to induce ciliogenesis, and finally processed for immunofluorescence or biochemistry.

### Fluorescence microscopy

For immunofluorescence, cells grown on coverslips were washed twice in PBS and fixed in methanol:acetone (1:1) at –20°C for 4 minutes or in 4% paraformaldehyde (PFA) for 20 minutes at 4°C followed by a 10 minute incubation in PBS-$NH_4Cl$ (50 mM). Cells were incubated with primary antibodies in PBS containing 0.1% Triton X-100 (Sigma) and 1 mg/ml bovine serum albumin (BSA) for 45 minutes at room temperature. After two washes with PBS-BSA, cells were incubated for 30 minutes at room temperature in PBS-BSA containing secondary antibodies. After one wash with PBS-BSA and two washes in PBS, cells were laid down plated on microscope slides in a PBS-glycerol mix (50:50) using the SlowFade Light Antifade Kit containing DAPI from Molecular Probes (S36938, Invitrogen). Samples were examined under an epi-illumination microscope (DMI 6000, Leica) with a cooled charge-coupled device (CCD) camera (MicroMax, Princeton Instruments). Images were acquired with MetaMorph (Molecular Devices) and processed with MetaMorph and Photoshop CS2 (Adobe Systems, San Jose, CA).

For 3D reconstruction, *Z*-stacks of epifluorescence images were obtained with an epi-illumination microscope (Axiovert 100M, Zeiss) using a piezoelectric 100× objective (plan-apo) enabling acquisition of images every 200 nm along the *Z*-axis. Deconvolution of *Z*-stacks was achieved with MetaMorph and 3D reconstruction of deconvoluted images with the Imaris software (Bitplane). Images were extracted from Imaris and then used to obtain the final images used in the figures.

For transferrin staining, RPE1 cells transfected with the GFP-F plasmid were first incubated for 20 minutes at 37°C in serum-free DMEM to eliminate receptor-bound endogenous transferrin. Cells were then washed twice in DMEM-BSA (1 mg/ml) and incubated for 1-3 minutes at 37°C in DMEM-BSA containing 6 μg/ml Alexa Fluor 545-conjugated transferrin. The cells were rapidly washed in cold PBS, fixed and processed for immunofluorescence as described above.

For dynamic analysis of clathrin or actin at the ciliary pocket, RPE1 cells grown on specific μ-slides (Ibidi) were co-transfected with both rab8-GFP and clathrin-DsRed or LifeAct-Cherry encoding plasmids, transferred to low-serum medium and analysed 24 or 48 hours later. Live-cell fluorescence microscopy was performed using an Apo 100× NA 1.43 microscope objective with an inverted epi-illumination microscope (Axiovert 100M, Zeiss) placed within a temperature-controlled enclosure set at 37°C. GFP and DsRed-cherry images were acquired successively every 3 seconds for 3-20 minutes. Shutters, filters, camera and acquisition were controlled by MetaMorph. The final movies and images were generated using Metamorph, ImageJ (http://rsbweb.nih.gov/ij/index.html) and Photoshop.

### Electron microscopy

For scanning electron microscopy, cells were washed in PBS, fixed for at least 1 hour with 2.5% glutaraldehyde in PBS or in 0.2 M cacodylate buffer, washed and post-fixed in 1% osmium tetroxide. After dehydration, samples were critical-point dried (Emitech K850 or Balzers UnionCPD30) and coated with gold (Jeol JFC-1200 or Gatan Ion Beam Coater 681). Samples were visualised with a Jeol JM6700 F scanning microscope.

For transmission electron microscopy (TEM), cells were grown on coverslips were fixed for 1 hour with 3% glutaraldehyde. Samples were post-fixed with 1% osmium tetroxide in 0.1 M phosphate buffer, then dehydrated in 70%, 90% and 100% ethanol. After 10 minutes in a 1:2 mixture of epoxy propane and epoxy resin, the cells were embedded in gelatin capsules with freshly prepared epoxy resin and polymerised at 60°C for 24 hours. Sections of 80 nm were cut with an ultramicrotome (Reichert ultracut S), stained with uranyl acetate and Reynold's lead citrate, and observed with a transmission electron microscope (Philips CM10).

The COCs were fixed in a 100 µl drop of 2.5% glutaraldehyde in Sorensen medium supplemented with 1% BSA for 30 minutes at room temperature and 1 hour at 4°C. After three washes in Sorensen with 1% BSA, the COCs were post-fixed, dehydrated and embedded in gelatin capsules with epoxy resin, as described above. Brains from P4, P14 and P21 mice were sectioned at 200 µm using a vibratome (VT 1200S, Leica). Sections of the rostral lateral wall of the lateral ventricle were dissected in PBS under a dissecting microscope. Ventricle slices were fixed in 2.5% glutaraldehyde and 4% PFA. Tissues were treated with 1% osmium tetroxide. Fixed specimens were washed and progressively dehydrated. Samples were then incubated in 1% uranyl acetate in 70% methanol and dehydrated again through a graded series of ethanol. Samples were pre-impregnated with ethanol:epon mix (2:1, 1:1, 1:2 ratios), and impregnated with epon. Samples were then mounted into epon blocks and 70 nm thin sections were cut, as described above.

### Immunoblotting

Cells were lysed by incubation in 0.02 M Tris-HCl, pH 7.5, 1% (v/v) NP40, 0.1 M $NH_4SO_4$, 10% glycerol (v/v), 10 mM protease inhibitor cocktail (Sigma) for 30 minutes at 4°C. After centrifugation (13,400 ***g***), cleared lysates were separated by polyacrylamide gel electrophoresis (SDS-PAGE) and transferred onto polyvinylidene fluoride transfer membranes (PVDF, GE Healthcare) using the NuPage electrophoresis system (Invitrogen). Immunoblotting was performed using the indicated primary antibodies and revealed using the ECL+ Detection Kit (GE Healthcare).

The authors would like to thank F. Niedergang, A. Touré, G. Bismuth, M. Bornens, A. Echard, G. Montagnac, J. Rappoport, E. Macia and M. Franco for reagents, stimulating discussions and advice; people from the 'Imagerie Cellulaire' facility of the Cochin Institute for their help; P. Attal for assistance with maths in supplementary material Fig. S3. The present work was partially funded by a grant from the ANR 'GENOPAT 2009' (R09088KS to S.S., A.B. and P.B.). Research at Institut Pasteur was funded by the Institut Pasteur and the CNRS.

Supplementary material available online at
http://jcs.biologists.org/cgi/content/full/123/10/1785/DC1

## References

**Allen, C. L., Goulding, D. and Field, M. C.** (2003). Clathrin-mediated endocytosis is essential in Trypanosoma brucei. *EMBO J.* **22**, 4991-5002.

**Benmerah, A. and Lamaze, C.** (2007). Clathrin-coated pits: vive la difference? *Traffic* **8**, 970-982.

**Bonhivers, M., Nowacki, S., Landrein, N. and Robinson, D. R.** (2008). Biogenesis of the trypanosome endo-exocytotic organelle is cytoskeleton mediated. *PLoS Biol.* **6**, e105.

**Borck, G., Molla-Herman, A., Boddaert, N., Encha-Razavi, F., Philippe, A., Robel, L., Desguerre, I., Brunelle, F., Benmerah, A., Munnich, A. et al.** (2008). Clinical, cellular, and neuropathological consequences of AP1S2 mutations: further delineation of a recognizable X-linked mental retardation syndrome. *Hum. Mutat.* **29**, 966-974.

**Brechbuhl, J., Klaey, M. and Broillet, M. C.** (2008). Grueneberg ganglion cells mediate alarm pheromone detection in mice. *Science* **321**, 1092-1095.

**Breunig, J. J., Sarkisian, M. R., Arellano, J. I., Morozov, Y. M., Ayoub, A. E., Sojitra, S., Wang, B., Flavell, R. A., Rakic, P. and Town, T.** (2008). Primary cilia regulate hippocampal neurogenesis by mediating sonic hedgehog signaling. *Proc. Natl. Acad. Sci. USA* **105**, 13127-13132.

**Chen, W., Ren, X. R., Nelson, C. D., Barak, L. S., Chen, J. K., Beachy, P. A., de Sauvage, F. and Lefkowitz, R. J.** (2004). Activity-dependent internalization of smoothened mediated by beta-arrestin 2 and GRK2. *Science* **306**, 2257-2260.

**Christensen, S. T., Pedersen, L. B., Schneider, L. and Satir, P.** (2007). Sensory cilia and integration of signal transduction in human health and disease. *Traffic* **8**, 97-109.

**Corbit, K. C., Aanstad, P., Singla, V., Norman, A. R., Stainier, D. Y. and Reiter, J. F.** (2005). Vertebrate Smoothened functions at the primary cilium. *Nature* **437**, 1018-1021.

**Dingemans, K. P.** (1969). The relation between cilia and mitoses in the mouse adenohypophysis. *J. Cell Biol.* **43**, 361-367.

**Fawcett, D. W., Eddy, E. M. and Phillips, D. M.** (1970). Observations on the fine structure and relationships of the chromatoid body in mammalian spermatogenesis. *Biol. Reprod.* **2**, 129-153.

**Field, M. C. and Carrington, M.** (2009). The trypanosome flagellar pocket. *Nat. Rev. Microbiol.* **7**, 775-786.

**Fonte, V. G., Searls, R. L. and Hilfer, S. R.** (1971). The relationship of cilia with cell division and differentiation. *J. Cell Biol.* **49**, 226-229.

**Gadelha, C., Rothery, S., Morphew, M., McIntosh, J. R., Severs, N. J. and Gull, K.** (2009). Membrane domains and flagellar pocket boundaries are influenced by the cytoskeleton in African trypanosomes. *Proc. Natl. Acad. Sci. USA* **106**, 17425-17430.

**Garcia-Salcedo, J. A., Perez-Morga, D., Gijon, P., Dilbeck, V., Pays, E. and Nolan, D. P.** (2004). A differential role for actin during the life cycle of Trypanosoma brucei. *EMBO J.* **23**, 780-789.

**Han, Y. G., Spassky, N., Romaguera-Ros, M., Garcia-Verdugo, J. M., Aguilar, A., Schneider-Maunoury, S. and Alvarez-Buylla, A.** (2008). Hedgehog signaling and primary cilia are required for the formation of adult neural stem cells. *Nat. Neurosci.* **11**, 277-284.

**Haycraft, C. J., Banizs, B., Aydin-Son, Y., Zhang, Q., Michaud, E. J. and Yoder, B. K.** (2005). Gli2 and Gli3 localize to cilia and require the intraflagellar transport protein polaris for processing and function. *PLoS Genet* **1**, e53.

**Herman, B. and Albertini, D. F.** (1983). Microtubule regulation of cell surface receptor topography during granulosa cell differentiation. *Differentiation* **25**, 56-63.

**Hinrichsen, L., Harborth, J., Andrees, L., Weber, K. and Ungewickell, E. J.** (2003). Effect of clathrin heavy chain- and alpha-adaptin-specific small inhibitory RNAs on endocytic accessory proteins and receptor trafficking in HeLa cells. *J. Biol. Chem.* **278**, 45160-45170.

**Huang, F., Khvorova, A., Marshall, W. and Sorkin, A.** (2004). Analysis of clathrin-mediated endocytosis of epidermal growth factor receptor by RNA interference. *J. Biol. Chem.* **279**, 16657-16661.

**Ihara, M., Kinoshita, A., Yamada, S., Tanaka, H., Tanigaki, A., Kitano, A., Goto, M., Okubo, K., Nishiyama, H., Ogawa, O. et al.** (2005). Cortical organization by the septin cytoskeleton is essential for structural and mechanical integrity of mammalian spermatozoa. *Dev. Cell* **8**, 343-352.

**Jensen, C. G., Poole, C. A., McGlashan, S. R., Marko, M., Issa, Z. I., Vujcich, K. V. and Bowser, S. S.** (2004). Ultrastructural, tomographic and confocal imaging of the chondrocyte primary cilium in situ. *Cell Biol. Int.* **28**, 101-110.

**Jurczyk, A., Gromley, A., Redick, S., San Agustin, J., Witman, G., Pazour, G. J., Peters, D. J. and Doxsey, S.** (2004). Pericentrin forms a complex with intraflagellar transport proteins and polycystin-2 and is required for primary cilia assembly. *J. Cell Biol.* **166**, 637-643.

**Kissel, H., Georgescu, M. M., Larisch, S., Manova, K., Hunnicutt, G. R. and Steller, H.** (2005). The Sept4 septin locus is required for sperm terminal differentiation in mice. *Dev. Cell* **8**, 353-364.

**Kreuzer, O. J., Krisch, B., Dery, O., Bunnett, N. W. and Meyerhof, W.** (2001). Agonist-mediated endocytosis of rat somatostatin receptor subtype 3 involves beta-arrestin and clathrin coated vesicles. *J. Neuroendocrinol.* **13**, 279-287.

**Macia, E., Ehrlich, M., Massol, R., Boucrot, E., Brunner, C. and Kirchhausen, T.** (2006). Dynasore, a cell-permeable inhibitor of dynamin. *Dev. Cell* **10**, 839-850.

**Mirzadeh, Z., Merkle, F. T., Soriano-Navarro, M., Garcia-Verdugo, J. M. and Alvarez-Buylla, A.** (2008). Neural stem cells confer unique pinwheel architecture to the ventricular surface in neurogenic regions of the adult brain. *Cell Stem Cell* **3**, 265-278.

**Molla-Herman, A., Boularan, C., Ghossoub, R., Scott, M. G., Burtey, A., Zarka, M., Saunier, S., Concordet, J. P., Marullo, S. and Benmerah, A.** (2008). Targeting of beta-arrestin2 to the centrosome and primary cilium: role in cell proliferation control. *PLoS ONE* **3**, e3728.

**Motley, A., Bright, N. A., Seaman, M. N. and Robinson, M. S.** (2003). Clathrin-mediated endocytosis in AP-2-depleted cells. *J. Cell Biol.* **162**, 909-918.

**Nachury, M. V., Loktev, A. V., Zhang, Q., Westlake, C. J., Peranen, J., Merdes, A., Slusarski, D. C., Scheller, R. H., Bazan, J. F., Sheffield, V. C. et al.** (2007). A core complex of BBS proteins cooperates with the GTPase Rab8 to promote ciliary membrane biogenesis. *Cell* **129**, 1201-1213.

**Nikai, H., Rose, G. G. and Cattoni, M.** (1970). Electron microscopy of solitary cilia in human gingiva and rat oral mucosa. *J. Dent. Res.* **49**, 1141-1153.

**Overath, P. and Engstler, M.** (2004). Endocytosis, membrane recycling and sorting of GPI-anchored proteins: Trypanosoma brucei as a model system. *Mol. Microbiol.* **53**, 735-744.

**Park, T. J., Mitchell, B. J., Abitua, P. B., Kintner, C. and Wallingford, J. B.** (2008). Dishevelled controls apical docking and planar polarization of basal bodies in ciliated epithelial cells. *Nat. Genet.* **40**, 871-879.

**Pazour, G. J., Dickert, B. L., Vucica, Y., Seeley, E. S., Rosenbaum, J. L., Witman, G. B. and Cole, D. G.** (2000). Chlamydomonas IFT88 and its mouse homologue, polycystic kidney disease gene tg737, are required for assembly of cilia and flagella. *J. Cell Biol.* **151**, 709-718.

**Pedersen, L. B. and Rosenbaum, J. L.** (2008). Intraflagellar transport (IFT) role in ciliary assembly, resorption and signalling. *Curr. Top Dev. Biol.* **85**, 23-61.

**Perrais, D. and Merrifield, C. J.** (2005). Dynamics of endocytic vesicle creation. *Dev. Cell* **9**, 581-592.

**Rappoport, J. Z., Taha, B. W., Lemeer, S., Benmerah, A. and Simon, S. M.** (2003). The AP-2 complex is excluded from the dynamic population of plasma membrane-associated clathrin. *J. Biol. Chem.* **278**, 47357-47360.

**Rappoport, J. Z., Simon, S. M. and Benmerah, A.** (2004). Understanding living clathrin-coated pits. *Traffic* **5**, 327-337.

**Riedl, J., Crevenna, A. H., Kessenbrock, K., Yu, J. H., Neukirchen, D., Bista, M., Bradke, F., Jenne, D., Holak, T. A., Werb, Z. et al.** (2008). Lifeact: a versatile marker to visualize F-actin. *Nat. Methods* **5**, 605-607.

**Scholey, J. M.** (2008). Intraflagellar transport motors in cilia: moving along the cell's antenna. *J. Cell Biol.* **180**, 23-29.
**Schulz, S., Handel, M., Schreff, M., Schmidt, H. and Hollt, V.** (2000). Localization of five somatostatin receptors in the rat central nervous system using subtype-specific antibodies. *J. Physiol. Paris* **94**, 259-264.
**Sharma, N., Berbari, N. F. and Yoder, B. K.** (2008). Ciliary dysfunction in developmental abnormalities and diseases. *Curr. Top Dev. Biol.* **85**, 371-427.
**Smith, J. W., Christie, K. N. and Frame, J.** (1969). Desmosomes, cilia and acanthosomes associated with keratocytes. *J. Anat.* **105**, 383-392.
**Sorokin, S.** (1962). Centrioles and the formation of rudimentary cilia by fibroblasts and smooth muscle cells. *J. Cell Biol.* **15**, 363-377.
**Sorokin, S. P.** (1968). Reconstructions of centriole formation and ciliogenesis in mammalian lungs. *J. Cell Sci.* **3**, 207-230.
**Spiliotis, E. T. and Nelson, W. J.** (2006). Here come the septins: novel polymers that coordinate intracellular functions and organization. *J. Cell Sci.* **119**, 4-10.
**Teilmann, S. C., Byskov, A. G., Pedersen, P. A., Wheatley, D. N., Pazour, G. J. and Christensen, S. T.** (2005). Localization of transient receptor potential ion channels in primary and motile cilia of the female murine reproductive organs. *Mol. Reprod. Dev.* **71**, 444-452.
**Vladar, E. K. and Axelrod, J. D.** (2008). Dishevelled links basal body docking and orientation in ciliated epithelial cells. *Trends Cell. Biol.* **18**, 517-520.
**Wheatley, D. N.** (1969). Cilia in cell-cultured fibroblasts. I. On their occurrence and relative frequencies in primary cultures and established cell lines. *J. Anat.* **105**, 351-362.
**Yoshimura, S., Egerer, J., Fuchs, E., Haas, A. K. and Barr, F. A.** (2007). Functional dissection of Rab GTPases involved in primary cilium formation. *J. Cell Biol.* **178**, 363-369.